INTERFACE

rsif.royalsocietypublishing.org

Research

Cite this article: Yigit B, Pekkan K. 2016 Non-dimensional physics of pulsatile cardiovascular networks and energy efficiency. *J. R. Soc. Interface* **13**: 20151019. http://dx.doi.org/10.1098/rsif.2015.1019

Received: 25 November 2015
Accepted: 4 January 2016

Subject Areas:
biomedical engineering, biomechanics, bioengineering

Keywords:
haemodynamics, comparative cardiovascular scaling, body size scaling, power loss

Author for correspondence:
Kerem Pekkan
e-mail: kpekkan@ku.edu.tr

Electronic supplementary material is available at http://dx.doi.org/10.1098/rsif.2015.1019 or via http://rsif.royalsocietypublishing.org.

THE ROYAL SOCIETY PUBLISHING

Non-dimensional physics of pulsatile cardiovascular networks and energy efficiency

Berk Yigit[1] and Kerem Pekkan[2,3]

[1]Department of Mechanical Engineering, and [2]Department of Biomedical Engineering, Carnegie Mellon University, Pittsburgh, PA, USA
[3]Department of Mechanical Engineering, Koç University, Istanbul, Turkey

BY, 0000-0002-3253-9452; KP, 0000-0001-7637-4445

In Nature, there exist a variety of cardiovascular circulation networks in which the energetic ventricular load has both *steady* and *pulsatile* components. Steady load is related to the mean cardiac output (CO) and the haemodynamic resistance of the peripheral vascular system. On the other hand, the pulsatile load is determined by the simultaneous pressure and flow waveforms at the ventricular outlet, which in turn are governed through arterial wave dynamics (transmission) and pulse decay characteristics (windkessel effect). Both the steady and pulsatile contributions of the haemodynamic power load are critical for characterizing/comparing disease states and for predicting the performance of cardiovascular devices. However, haemodynamic performance parameters vary significantly from subject to subject because of body size, heart rate and subject-specific CO. Therefore, a 'normalized' energy dissipation index, as a function of the 'non-dimensional' physical parameters that govern the circulation networks, is needed for comparative/integrative biological studies and clinical decision-making. In this paper, a complete network-independent non-dimensional formulation that incorporates pulsatile flow regimes is developed. Mechanical design variables of cardiovascular flow systems are identified and the Buckingham Pi theorem is formally applied to obtain the corresponding non-dimensional scaling parameter sets. Two scaling approaches are considered to address both the lumped parameter networks and the distributed circulation components. The validity of these non-dimensional number sets is tested extensively through the existing empirical allometric scaling laws of circulation systems. Additional validation studies are performed using a parametric numerical arterial model that represents the transmission and windkessel characteristics, which are adjusted to represent different body sizes and non-dimensional haemodynamic states. Simulations demonstrate that the proposed non-dimensional indices are independent of body size for healthy conditions, but are sensitive to deviations caused by off-design disease states that alter the energetic load. Sensitivity simulations are used to identify the relationship between pulsatile power loss and non-dimensional characteristics, and optimal operational states are computed.

1. Introduction

The human circulation system, with its four-chambered heart, has been rigorously studied; however, it is not the only possible working configuration present in Nature. There are a great variety of circulation systems that exhibit peculiar haemodynamics and diverse energetic performance, because of the arbitrary numbers and orientation of ventricles [1,2], auto-regulated shunts [3–5] and exotic cardiovascular valve designs [6–9] that address oxygen and nutrition transport [10–12]. For improved cardiac filling, even at ultra-low venous pressures, special mechanisms are employed, such as booster pumps [13] in the hagfish heart and stiff pericardium translating the ventricular

contraction to venous suction in the auricles of bivalve molluscs [14] and insects [15]. Both of these examples have 'open' circulation systems.

Despite numerous biological reports on the circulation systems of various species, major variations in their cardiovascular parameters, such as organism size, network arrangement, flow pulsatility, vascular material properties and cardiac output (CO) level, significantly challenge an elegant *comparative* analysis across the phylogenetic spectrum. This poses a barrier to the translation of ideas from Nature to technology, and hinders our fundamental and clinical comprehension of cardiovascular systems. Therefore, in this paper, a general unifying engineering framework is developed to compare haemodynamics, functional component designs (i.e. valves, shunts and junctions) and the energy cascades encountered in these alternative circulation system networks.

A formal hydrodynamic non-dimensionalization [16,17] of cardiovascular circuits has yet to be performed. Thus, starting with a systematic application of similitude principles, we proposed alternative non-dimensionalization schemes that address the intra- and inter-species variations of cardiovascular parameters. The present approach is based on a recent methodology, developed by our group, which covers the non-dimensional analysis of steady energy dissipation (i.e. power scaling) in any component (vessels and ventricles) of the circulatory system, and formulates the full energy budget for venous and arterial circulations [18,19]. This approach allowed disease-specific subject-to-subject comparisons and disease-to-disease evaluations by quantifying the haemodynamic severity of one vascular disease type versus another, or at different time points for the same disease [20]. In this paper, for the first time, we have formulated additional non-dimensional indices that govern vascular compliance, heart rate, wave reflections and the cardiac-cycle pulsatility. Furthermore, this complete non-dimensional parameter set is integrated in the reduced-order lumped parameter network models (LPMs) of general circulation systems, making our approach independent of the cardiovascular system network.

We hypothesize that establishing the similitude conditions of the pulsatile cardiovascular flow networks will advance our understanding of cardiovascular disease states [21–23], and will influence the haemodynamic design of blood-wetted devices. For example, during cardiopulmonary bypass (CPB), the haemodynamic energy delivered to the peripheral organs can be modulated by manipulating the pulsatile flow waveform while delivering the same net perfusion flow rate through the aortic CPB cannula [24]. However, appropriate energy efficiency indices, which incorporate patient size and circulation network parameters, are not available to improve such device systems. The need for similar indices that can quantify and compare the pulsatile energetic load in cardiovascular disease [21], in the exercise performance of a patient with a single ventricle [25], in CPB [26,27], in heart valves [28,29] as well as in total cavo-pulmonary connection surgery [30,31], prompted the present detailed investigation. Likewise, to address clinical needs, various pulsatile flow indices have been proposed. For example, Shepard *et al.* [32] defined the energy equivalent pressure (EEP = total haemodynamic work/net flow rate) to quantify the energetic cost of pulsatile haemodynamic flow that differed from the steady load. Even though EEP is useful to assess the relative cost of pulsatile flow, it does not explain the physical factors that determine the pulsatile load, nor the relation of energetic cost to patient size. As the haemodynamic energy dissipation is a body size-dependent quantity, and varies significantly from patient to patient, scaling and normalization of energetic dissipation is essential for comparative clinical analysis [33].

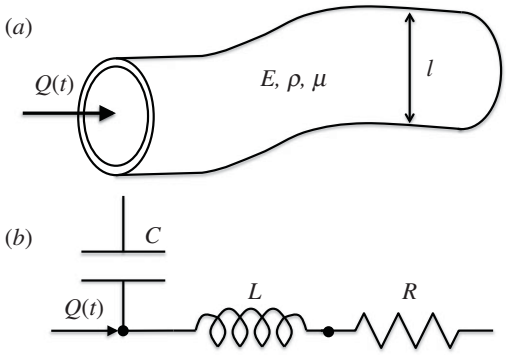

Figure 1. (*a*) A general three-dimensional one inlet–one outlet pulsatile vascular component is described by its physical parameters: fluidic density ρ, viscosity μ, wall elastic modulus E, characteristic length l and the flow rate $Q(t)$. (*b*) The same vascular segment described in the lumped element domain. Elastic, inertial and viscous properties are represented by compliance C, inertance L and resistance R. The characteristic length, l, is related to the body surface area of the species, as described in the text.

In summary, through application of the present framework, we provide physics-based scaling indices and conduct characterization studies of the circulatory function and its associated energetic cost based on the proposed dimensionless numbers that govern pulsatile haemodynamics.

2. Methodology

2.1. Steady and pulsatile energy dissipation

The mean pulsatile energy dissipation rate ($\bar{\varepsilon}_{\mathrm{p}}$) is the difference between the mean total energy dissipation rate ($\bar{\varepsilon}_{\mathrm{T}}$) and the energy dissipation rate of the steady component of the flow ($\bar{\varepsilon}_{\mathrm{s}}$),

$$\bar{\varepsilon}_{\mathrm{p}} = \bar{\varepsilon}_{\mathrm{T}} - \bar{\varepsilon}_{\mathrm{s}} = \frac{1}{T}\oint p(t)q(t)\mathrm{d}t - \frac{1}{T^2}\oint p(t)\,\mathrm{d}t \oint q(t)\,\mathrm{d}t, \qquad (2.1)$$

where $p(t)$ and $q(t)$ are instantaneous pressure and flow rate at the junction of the aorta and ventricle, respectively, and T is the duration of the cardiac cycle. The vascular structural properties and network configuration determine the pressure-flow waveforms in each vascular segment through pulse wave propagation and damping, which consequently determine the energetic load.

2.2. Similitude of pulsatile flow in compliant vessels

A theoretical analysis of haemodynamic power loss under non-pulsatile flow conditions has recently been provided by Dasi *et al.* [18,19]. Expanding this formulation to pulsatile flow regimes, we start by describing a vascular 'compartment' as a physical model of an isolated segment of the flow system in which the flow is governed by the physical properties and geometry of the flow domain, in addition to the physical conditions imposed at its boundaries (figure 1). In §2.2.1, the non-dimensional formulation of the flow dynamics in a distributed model of the vascular compartment is presented (figure 1*a*). In addition, an equivalent non-dimensional number set, which is motivated by the circulatory lumped parameter networks, is developed in §2.2.2 (figure 1*b*). In §2.2.3, we define a power

loss index (PLI), which weighs the power loss in a vascular segment against a subject-specific power scale.

2.2.1. Non-dimensionalization of distributed vascular component models

The physical parameters defining a vascular compartment are: blood density ρ, dynamic viscosity μ, vascular elastic modulus E, characteristic length l and its geometry, which is represented by a dimensionless form vector S containing ratios of lengths, as shown in figure 1*a*. At the inlet boundary, a pulsatile flow $Q(t)$ is imposed, which is characterized by its mean $\bar{Q}$, fundamental frequency (i.e. heart rate (HR)—in units of frequency) and waveform shape (spectral components of the waveform are included in a dimensionless vector Q_ω; electronic supplementary material, appendix A). Outlet boundary conditions (BCs) can range from simple constant pressure outlets to more complex windkessel (WK) outlets, one-dimensional distributed distal flow models or three-dimensional models. In the present formulation, all parameters related to outlet BCs are contained in a dimensionless 'β' vector (e.g. $\beta = P_o/(\rho\bar{Q}^2/l^4)$ for a constant pressure outlet).

The functional dependence of local pulsatile haemodynamic power loss ($\bar{\varepsilon}_p$) on these physical independent variables can be re-posed as a relationship between seven non-dimensional groups using the Buckingham Pi theorem (electronic supplementary material, appendix B):

$$\frac{\bar{\varepsilon}_p}{\rho(\bar{Q}^3/l^4)} = f\,(Re, Ca, St, Q_\omega, S, \beta), \tag{2.2a}$$

where

$$Re = \frac{\rho\bar{Q}/l}{\mu}, \quad Ca = \frac{E}{\rho\bar{Q}^2/l^4} \quad \text{and} \quad St = \frac{\mathrm{HR}}{\bar{Q}/l^3}, \tag{2.2b}$$

and where Re is the Reynolds number, Ca is the Cauchy number and St is the Strouhal number. Ca is the ratio of characteristic elastic force due to wall distension to the characteristic dynamic forces inside the flow. St is the ratio of oscillatory time to characteristic flow time. The left-hand side of equation (2.2*a*) is the ratio of pulsatile power loss to a characteristic inertial power that is flowing into the compartment. For 'compliant' arteries, veins and pulmonary microcirculation, the effect of gravity can be significant; the inclusion of gravity (g) in the analysis would require the Froude number ($Fr = \bar{Q}/\sqrt{g}l^{5/2}$) to be included in equation (2.2) and the vascular orientation (or posture) to be considered in the shape parameter vector S.

2.2.2. Non-dimensionalization of lumped vascular component models

While the previous non-dimensional number set governs the pulsatile flow physics for a compartment, completely, an alternative similitude set would be more amenable for circulation network analysis. Particularly for complex vascular systems consisting of many vessels and vascular components, it may not be practical to individually consider the contribution of each element to the vascular function. Instead, the lumped haemodynamic parameters, resistance (R), compliance (C) and inertance (L), incorporate the effect of material properties (viscous, elastic and inertial, respectively) and the prevailing geometry in a single parameter that represents the haemodynamic function of the specific vascular segment that is under consideration (figure 1*b*). Our intention here is to develop 'non-dimensional' circulation networks and to be able to compare them through numerical LPMs. While higher-order analysis methods of cardiovascular systems do exist, we find LPMs to be the most practical approach, leading to a system-level understanding [34].

For a lumped compartment, the functional dependence of the mean pulsatile energy dissipation on the independent lumped variables is represented by $\bar{\varepsilon}_p = f\,(R, C, L, \mathrm{HR}, \bar{Q}, Q_\omega, S, \beta)$. Following non-dimensionalization (electronic supplementary material, appendix C), the functional dependence of $\bar{\varepsilon}_p$ can be re-posed as a function of six dimensionless quantities:

$$\frac{\bar{\varepsilon}_p}{R\bar{Q}^2} = f\,(\delta, \psi, Q_\omega, S, \beta), \tag{2.3a}$$

where

$$\delta = \frac{1}{\mathrm{HR} \times RC}, \quad \psi = \mathrm{HR}\sqrt{LC}. \tag{2.3b}$$

Equation (2.3*a*) gives the ratio of pulsatile power loss to the steady power loss ($= R\bar{Q}^2$), as a function of δ, the pulse decay number, and ψ, the wave propagation number. δ is based on the elastic and viscous components of a vascular segment, and governs the rise and decay characteristics of pressure in RC circuits, similarly to the WK model of circulation. ψ is based on the elastic and inertial components of a vascular segment, and governs the transmission of pulse waves across a given vascular segment that is characteristic of the transmission line model of the arterial system. Although the geometry is intrinsic to lumped parameters, S is kept in the formulation to relate the local geometrical information (e.g. the constriction in a stenotic artery) to the changes in R, L and C, if this relation is available.

2.2.3. Pulsatile power loss index: scaling with body size and cardiac output

Scaling of power loss with the body surface area (BSA) is critical for understanding the relation of energetics to body size and metabolism, which is imperative in biological and clinical contexts. In general, human and mammalian circulation exhibit geometrical similarity, and it has been shown that $l \sim \sqrt{\mathrm{BSA}}$ is an acceptable approximation for all major vessels [35,36]; thus, the characteristic length for the circulation is chosen as $\sqrt{\mathrm{BSA}}$. Similarly, the characteristic flow rate for the whole circulation is the CO. We define the PLI in any vascular compartment as the ratio of $\bar{\varepsilon}_p$ to the characteristic inertial power available in the circulation system, which is based on $\sqrt{\mathrm{BSA}}$ and CO, by manipulating equations (2.2*a*) and (2.3*a*), respectively, giving

$$\mathrm{PLI} = \frac{\bar{\varepsilon}_p}{\rho\mathrm{CO}^3/\mathrm{BSA}^2} = \alpha^3\left(\frac{\mathrm{BSA}^2}{l^4}\right) f\,(Re, Ca, St, Q_\omega, S, \beta) \tag{2.4a}$$

and

$$\mathrm{PLI} = \alpha^2 \mathrm{RI} g(\delta, \psi, Q_\omega, S, \beta), \tag{2.4b}$$

where $\alpha = \bar{Q}/\mathrm{CO}$ is the fraction of local flow to the total available flow and $\mathrm{RI} = R/(\rho\mathrm{CO}/\mathrm{BSA}^2)$ is the resistance index. In this report, the PLI is used as the measure of pulsatile energetic performance. In our earlier study, a 'steady flow' version of the PLI, where $\bar{\varepsilon}_s$ replaces $\bar{\varepsilon}_p$, has been used to assess total cavo-pulmonary conduit performance [19,25]. For presentation purposes, and in order to obtain practical clinically relevant value ranges, the PLI and RI are multiplied by 10^{-9} in this paper [18].

2.3. Arterial model

To experiment with these new non-dimensional indices, we developed a numerical model of the systemic arterial circulation. Figure 2 depicts the model of systemic arterial circulation that was used in parametric simulations to determine the changes in PLI with respect to the cardiovascular non-dimensional parameters. The model consists of a one-dimensional transmission line model of the aorta that terminates with a three-element windkessel (WK3) model of the peripheral microvasculature. C_a and L_a are the aortic compliance and inertance, C_p and R_p are the peripheral compliance and resistance, and $Z_c = \sqrt{L_a/C_a}$ is the characteristic impedance of the WK3. Arterial model parameters match the characteristics of adult

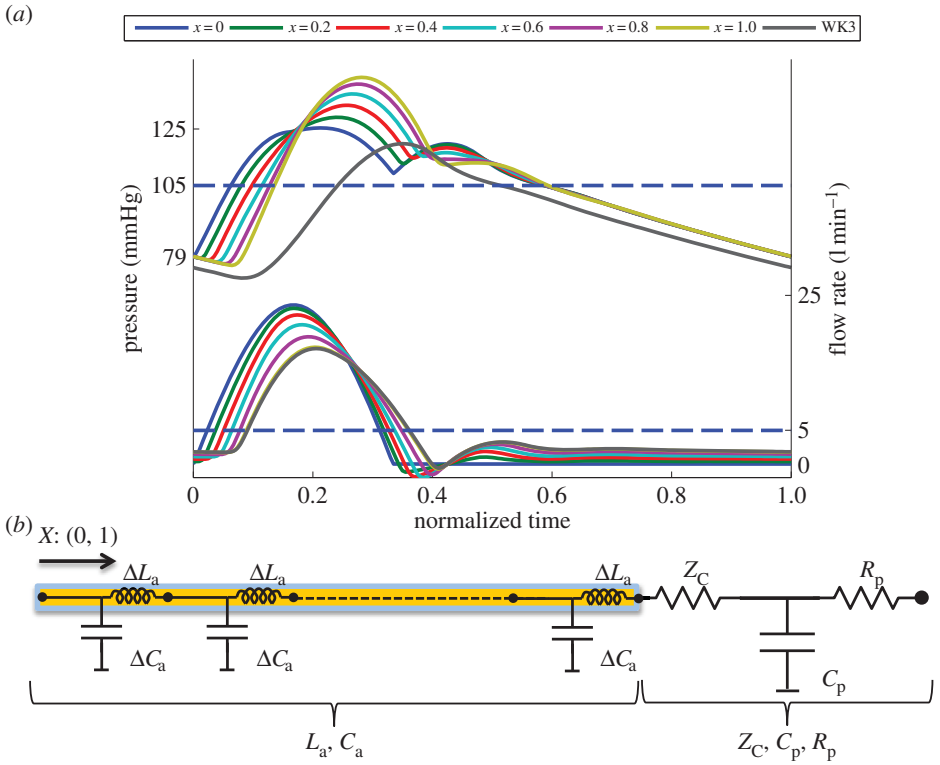

Figure 2. A sketch of the computational arterial model in the lumped element domain (*b*) and simulated arterial pressure and flow waveforms at the baseline model specifications representative of an adult with a body surface area of 1.5 m^2 (*a*). The model consists of a one-dimensional (1D) large arterial segment, similar to an aorta, which is terminated with a three-element windkessel (WK3), representing the peripheral microcirculation. *X* is the normalized distance ($\in (0, 1)$) from the inlet of the aorta to the major reflection site at the end of the aorta. Normalized time = *t*HR; in this particular simulation HR = 80 bpm. *t*, time; HR, heart rate; L_a, arterial inertance; C_a, arterial compliance; Z_C, arterial characteristic impedance ($= \sqrt{L_a/C_a}$); C_p, peripheral compliance; R_p, peripheral resistance. (Online version in colour.)

Table 1. Baseline systemic arterial model parameters and their units.

L_a	0.002	mmHg l^{-1} min^2	R_p	18.75	mmHg l^{-1} min
C_a	0.00042	$mmHg^{-1}$ l	HR	80	min^{-1}
Z_C	2.2	mmHg l^{-1} min	CO	5	l min^{-1}
C_T	0.001	$mmHg^{-1}$ l	BSA	1.5	m^2

human circulation (table 1) [37]. The arterial segment is uniform; therefore, wave reflections occur only at the intersection of the arterial segment and the WK3. This is a simplification of the actual system, which contains spatially distributed wave reflections; however, the focal point of combined wave reflections can be approximated as a single site [38]. To represent a healthy physiology, the characteristic impedance of the WK was matched to the characteristic impedance of the aorta ($Z_C = \sqrt{L_a/C_a}$) in order to minimize wave reflections at high frequencies [37,39,40]. The inlet BC is prescribed as a half sine pulsatile flow waveform, with $\bar{Q} = 5\,l\,min^{-1}$ and a systolic fraction of $t_{sys} = 0.3/HR$. The outlet BC is prescribed as zero pressure. Details of the computational model are discussed in the electronic supplementary material, appendix D. Figure 2 shows arterial pressure and flow waveforms sampled along different sites in the model, which showed realistic patterns such as the amplification of the pressure pulse in the direction of flow, a dicrotic notch and backwards flow in the aorta at the end of the ventricular ejection [39].

The complete arterial system (either systemic or pulmonary) can be considered as a single cardiovascular compartment based on the model presented above. Based on our numerical experiments, WK properties are governed by R_p, total arterial compliance ($C_T = C_a + C_p$), and HR, which gives the non-dimensional δ number of the arterial system: $\delta = (HRC_TR_p)^{-1}$. Similarly, pulse transmission characteristics are governed by the propagation number of the arterial compartment: $\psi = HR\sqrt{L_aC_a}$. RI is calculated as $R_p/(\rho CO/BSA^2)$. As such, the PLI is calculated from the pulsatile power loss, CO and the BSA. The α term is dropped for one-compartment systems because $\bar{Q} = CO$.

Characteristic impedance Z_C does not show up in the non-dimensional numbers set, as it is not an independent parameter for the model under consideration at this time. Waveform shape is held constant across simulations; therefore, Q_ω does not change, and this term is subsequently dropped from the power loss function. Similarly, shape-related parameters (e.g. C_a/C_p) are held constant and *S* is excluded from the power loss function for simplicity, thereby assuming that the geometrical effects on energy loss, such as curvatures [41] and angles at branching junctions [42], are not drastically different between subjects. Geometrical effects introduced by stenoses, aneurysms and congenital defects are significant for haemodynamic losses in many cardiovascular diseases [21] and surgical reconstructions [20]; however, their investigation is outside the scope of the present study. Considering the above, the functional dependence of the PLI on non-dimensional parameters is given in

$$\mathrm{PLI} = \mathrm{RI}f(\delta, \psi). \tag{2.5}$$

As illustrated in this section, the proposed framework can be applied to any chosen cardiovascular compartment subset in a similar fashion.

Table 2. Allometric exponential coefficients of cardiovascular systems.

	surface-area scaling	quarter-power scaling	
	human [35][a]	mammals [43,47]	mammals [46]
aortic pressure	0	0	0
cardiac output	2/3	3/4	3/4
heart rate	−1/3	−1/4	−1/4
stroke volume	1	1	1
characteristic velocity	0	0	1/12
vascular dimensions	1/3	3/8	1/3
blood volume	1	1	1
total vascular resistance[b]	−2/3	−3/4	−3/4
total vascular compliance[b]	1	1	1
total arterial inertance[b]	−1/3	−1/2	−1/2

[a]Note that allometric functions based on body surface area (BSA) are converted to body volume relations by multiplying the allometric exponent for BSA by two-thirds under the observation that BSA scales with two-thirds of the body weight.
[b]The exponential coefficients for lumped parameters are estimated from the allometric relations reported in [35,43,46].

3. Results

3.1. Validation of pulsatile similitude via allometric relations

Allometric relations are statistically obtained power-law relations of the form $Y = aB^b$ that relate the value of a physiological parameter (Y) to body size (B) with a scaling exponent b and a normalization constant a. Allometric relations do not explain the variation of a variable for subjects with the same body sizes, but as it represents the statistical average of a large population, an allometrical trend can be interpreted as a 'normal' ball-park value for a physiological measure as a function of body size [33].

It is widely accepted that the relation between the size and form of efficient transportation networks dictates the allometric scaling of physiological variables with body mass M (i.e. $Y \sim M^b$), as shown through analytical models [43–46] and supported by empirical studies [35,47]. Observed values of b generally appear as multiples of 1/4 and 1/3, and are, respectively, attributed to the fractal and Euclidean scaling of geometry in biological organisms [48–50].

In this section, we propose that non-dimensionalized circulatory systems should yield scale-invariant characteristics, if their design is governed by a common optimality principle. For this purpose, we tested the proposed non-dimensional parameters for similitude (scale invariance) by the application of allometric relations for mammals (table 2) [35,43,45–47]. Two scaling schemes are considered in this study: quarter-power and surface-area scaling schemes, which are based on the empirically observed scaling of basal metabolic rate with body mass increased to the power of three-quarters and two-thirds; the former is commonly accepted in biological sciences, whereas the latter is accepted in the clinical field. Parameters not included in table 2 are the haemorheological properties (viscosity and density) and wall elastic modulus, which do not show a significant association with body size [48–50]. Normalized flow waveform shape, given by Q_ω, is considered to be independent of body size, as normalized ventricular contraction patterns and arterial flow waveforms are closely similar in mammals [51].

Allometric equations for similitude parameters governing local flow dynamics in a single conduit vessel component can be computed as

$$Re \propto M^{1/3},\ Ca \propto M^0 \text{ and } St \propto M^0 \text{ (surface-area scaling)}$$
$$Re \propto M^{5/12},\ Ca \propto M^{-1/6} \text{ and } St \propto M^0 \text{ (quarter-power scaling).}$$

Although there is geometrical similarity in the large vessels of an animal (i.e. $S \propto M^0$), as expected, only the dynamic similarity is not conserved, as inertial forces become dominant over viscous forces as the subject size increases.

Scaling of a single vessel gives an incomplete picture for the scaling of circulation as a system. To explore similitude in the entire circulation network, we refer to the scaling of the arterial system as a whole. We direct our attention to the most important aspects of pulsatile flow: frequency-dependent pulse propagation, damping and reflection, which can be adequately captured by the arterial model explained in §2.3. Allometric scaling of resistance, compliance and inertance can be determined empirically, or can be derived from the models of the underlying vascular structures (table 2). The body size proportionality of biological flow indices is determined from the above-mentioned allometric relations as:

$$\mathrm{RI} \propto M^0,\quad \delta \propto M^0 \quad \text{and} \quad \psi \propto M^0 \quad \text{(surface-area scaling)}$$
$$\mathrm{RI} \propto M^{-1/6},\ \delta \propto M^0 \quad \text{and} \quad \psi \propto M^0 \quad \text{(quarter-power scaling).}$$

The exponential coefficients for δ and ψ are zero, indicating that the non-dimensional parameters governing the pulsatile system are size invariant. It should be noted that the exponential scaling of the RI in the quarter-power scaling case does not break the generality of this finding, as it is not essentially a similitude parameter, but rather adjusts the proportionality of the PLI. As such, the exponential coefficient for the PLI is expected to be less than 0 (surface-area scaling), and greater than or equal to −1/6 (quarter-power scaling).

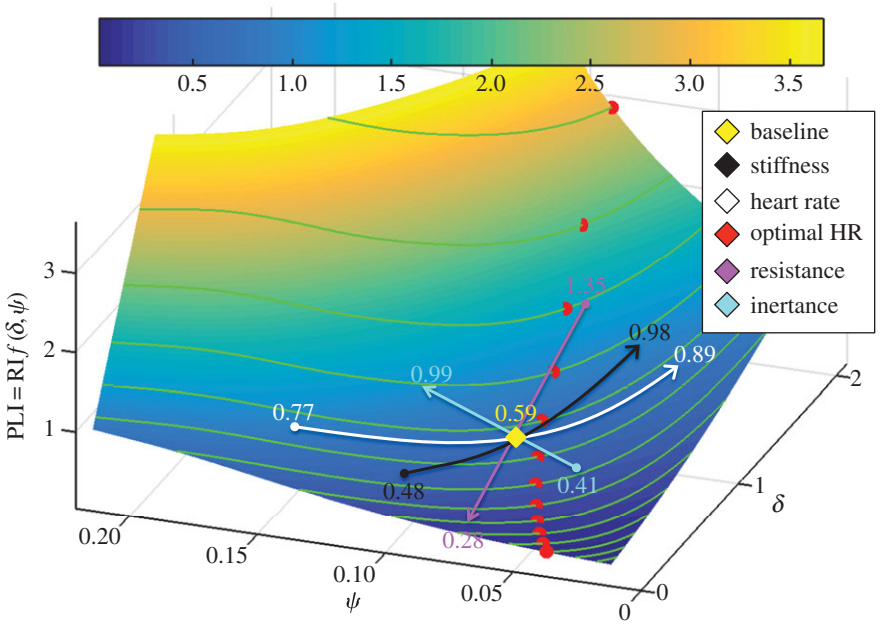

Figure 3. All possible haemodynamic states of a mammalian cardiovascular system represented through the non-dimensional parameters. Pulsatile PLI is plotted versus changes in propagation number ($\psi = \mathrm{HR}\sqrt{L_a C_a}$) and decay number ($\delta = 1/(\mathrm{HR} R_p C_T)$) at constant resistance index ($\mathrm{RI} = 10^{-9} R_p/(\rho \times \mathrm{CO} \times \mathrm{BSA}^{-2}) = 3.85$). Baseline condition (yellow marker, diamond) represents the systemic arteries of a healthy adult human that yields PLI = 0.59 at (δ, ψ) : (0.7, 0.074). The effects of changing a single cardiovascular parameter while keeping other non-dimensional numbers constant on the PLI are plotted as coloured curves, starting from half of the baseline parameter value (dot), passing from the baseline condition and ending at the tip of the arrow, at double its baseline value. Green curves on the surface represent constant vascular states ($\delta \times \psi = constant$); for each vascular state an optimal (δ, ψ) pair is computed (red markers, closed circles), where the PLI is at a local minimum. The colour legend shown on top corresponds to the value of the PLI. HR, heart rate; L_a, arterial inertance; C_a, arterial compliance; C_T, total compliance; R_p, peripheral resistance; ρ, blood density; CO, cardiac output; BSA, body surface area.

Therefore, the presented results confirm the validity of system-level similitude of the mammalian circulatory system when, regardless of the empirical scaling law options, non-dimensional parameters are formed with appropriately chosen length and time scales. The size-invariance property of non-dimensional characteristics enables the direct comparisons of cardiovascular operational and performance states to be made between different subjects.

3.2. Generalized pulsatile flow characteristics of the arterial system

In the present section, the variability in energetic characteristics that may accompany deviations from normal states is inspected as a function of similitude parameters using the parametric numerical model of the arterial system, as described in the Methodology (§2.3).

3.2.1. Pulsatile power loss index as a function of propagation and decay numbers

In this section, we inspect the impact of variations in propagation and damping characteristics governed by ψ and δ on the PLI, while isolating these effects from the mean resistive effects by fixing the value of the RI during simulations. The functional dependence of the PLI on δ and ψ, while the RI is held constant at 3.85, is displayed as a surface graph in figure 3. The 'baseline state' is defined as the arterial model for a healthy adult human, as described in §2.3. At this baseline state of the circulatory system, δ and ψ are 0.7 and 0.074, respectively, and the resulting PLI is 0.6. δ and ψ are both varied between 25% and 400% of their baseline values, and changes in the PLI are plotted on the state surface of figure 3. The PLI increases monotonically with both δ and ψ. Alternately doubling and then halving δ, while keeping the other non-dimensional parameters constant, resulted in a PLI of 1.4 (+127% change) and 0.3 (−54%), respectively. The same changes in ψ resulted in a PLI of 1.8 (+200%) and 0.3 (−50%), respectively. Simultaneously increasing or decreasing δ and ψ amplified the change in the PLI. No local extrema were observed in the power loss function.

The effects of changes in a single parameter (HR, R, L or C) are also plotted in figure 3. It was found that PLI increased with an increase in stiffness or inertance. PLI also increased with either a decrease or an increase in HR, indicating that a minimal PLI exists at an intermediate HR. An increase in R led to a decrease in PLI due to increased WK performance, even when the RI is allowed to increase. However, the total power loss significantly increased because of the steady component. The impact of changes in individual vascular properties over the PLI is further discussed in §4.1 and summarized in table 3.

One case that is worthy of investigation is the dependence of the PLI on the variability of the heart rate while the parameters depending on vascular properties (R, L, C) are held constant. This case is clinically interesting because the heart rate is a typical, acutely controlled system parameter, as opposed to the vascular geometry and material properties, which can be altered through long-term remodelling and growth processes. This observation leads to the constraint of acutely fixed vascular states, where only changes in heart rate are allowed. These iso-contours are displayed in figure 3, on curves defined as $\delta \times \psi = \sqrt{(L/C)}/R = k$, where k is a constant. The PLI is observed to increase with k, when RI is unchanged. Under the constraint of fixed vascular state, an optimal (δ, ψ) pair exists for each 'k', at which point the PLI reaches a local minimum. As observed, the simulated baseline (i.e. healthy) circulatory model was very close to the optimal condition,

Table 3. Influence of vascular properties on expected power loss through linear and nonlinear mechanisms. Combination of linear effects (propagation, damping, mean resistance), estimated by the arterial model, are given as overall influence on power loss. Sign of arrows indicates increasing or decreasing values; the implication for power loss is stated as favourable/unfavourable for a given flow rate. *Ma*, Mach number; *Re*, Reynolds number; ψ, propagation number; δ, decay number; RI, resistance index; *V*, volume; A_0, luminal area; *l*, length; ρ, density; μ, viscosity; *E*, elastic modulus; HR, heart rate; *Q*, flow rate; *U*, flow velocity; PWV, pulse wave velocity; *R*, lumped resistance; *C*, lumped compliance; *L*, lumped inertance.

		variation in vascular properties											
	governing parameter	↗ A_0		↗ *E*		↗ *R*		↗ *C*			↗ *L*		
steep wavefronts	*Ma*: $\frac{U}{PWV} \propto \frac{Q}{\sqrt{E/\rho}A_0}$	↘ *Ma* (favourable)		↘ *Ma* (favourable)		—		—			—		
turbulence	*Re*: $\frac{\rho Q/\sqrt{A_0}}{\mu}$	↘ *Re* (favourable)		—		—		—			—		
volume	$V = A_0 l$	↗ *V* (unfavourable)		—		—		—			—		
propagation	ψ	—	overall	↘ ψ (favourable)	overall	—	overall	↗ ψ (unfavourable)	overall	overall	↗ ψ (unfavourable)	overall	overall
damping	δ	↗ δ (unfavourable)	favourable	↗ δ (unfavourable)	unfavourable	↘ δ (favourable)	unfavourable	↘ δ (favourable)	favourable		—		unfavourable
mean resistance	RI	↘ RI (favourable)		—		↗ RI unfavourable)		—			—		

implying that human arterio-ventricular coupling is maintained close to an optimal state for a normal subject.

Figure 4*a*,*b* shows the pulsatile power loss as a fraction of the total power loss, which is 13% at the baseline, and increases with both δ and ψ. We observed that pulsatile power loss might surpass steady power loss under extreme cases. In figure 4*b*, a 'normal resting condition' region is enclosed by an approximate formula $\psi + 0.12\delta < 0.18$, inside which the pulsatile power loss as a fraction of the total power loss is below 20%, which is expected for normal resting subjects [52].

We have also investigated the changes in heart rate and vascular properties during exercise based on previously published data [53,54] (electronic supplementary material, appendix E, tables S1 and S2). During exercise, arterio-ventricular coupling is maintained at optimal (δ, ψ) states through balanced haemodynamic changes in HR, C_T and R_p (electronic supplementary material, figure S1). From rest to mild exercise, the PLI decreases by approximately 30%, but remains unchanged from mild to heavy exercise. However, the pulsatile power loss as a fraction of the total power loss increases from 13% at rest to approximately 30% during mild exercise and up to approximately 50% during heavy exercise.

3.2.2. Arterial pressure waveform as a function of propagation and decay numbers

Figure 5 shows the change in the normalized pulsatile pressure waveform at the inlet with respect to changes in δ and ψ. An increase in δ is reflected in the separation of systolic and diastolic pressures, indicating that the damping factor of the WK property is diminished (figure 5*a*). The slope of the diastolic pressure decay strongly correlates with the δ number. The arrival time of backwards travelling waves, originating from the arterial–peripheral boundary, increases in relation to the propagation number ψ, but not to δ. Increasing ψ, while keeping δ and RI constant, led to the observation that early arterial pulse pressure increases in relation to aortic impedance ($=\sqrt{L_a/C_a}$), which relates the instantaneous pressure and flow rate of the arterial pulse wave, thereby increasing the power requirement by the ventricle (figure 5*b*). It is also observed that the arterial model increasingly behaves as a classical *RC*-WK as ψ decreases [55]. The occurrence of an optimal state at an intermediate (δ, ψ) pair value, when the vascular state is fixed and either ψ or δ is varied, is also evident in figure 5*c*: at a high ψ (low δ), WK pressures are low but high pressures are required for generating the forward travelling pulse; on the contrary, WK losses are significant at low ψ (high δ).

3.3. Compartmentalization and non-dimensionalization of a general circulatory network

While the dimensionless relations shown in equations (2.2)–(2.4) are general, their physical role in a multi-component circulatory network system needs to be clarified. In our approach, any circulatory network can be divided into imaginary compartments and the connection map among these compartments can be determined. For example, figure 6 showcases the 'compartmentalization' scheme of sample complex circulation networks: crocodile and octopus [56–58]. Individually, each of these compartments may consist of one or more lumped elements, hierarchical, multi-scale, one-dimensional or three-dimensional distributed models. There is no restriction on the model being open or closed. In open models, BCs, and in

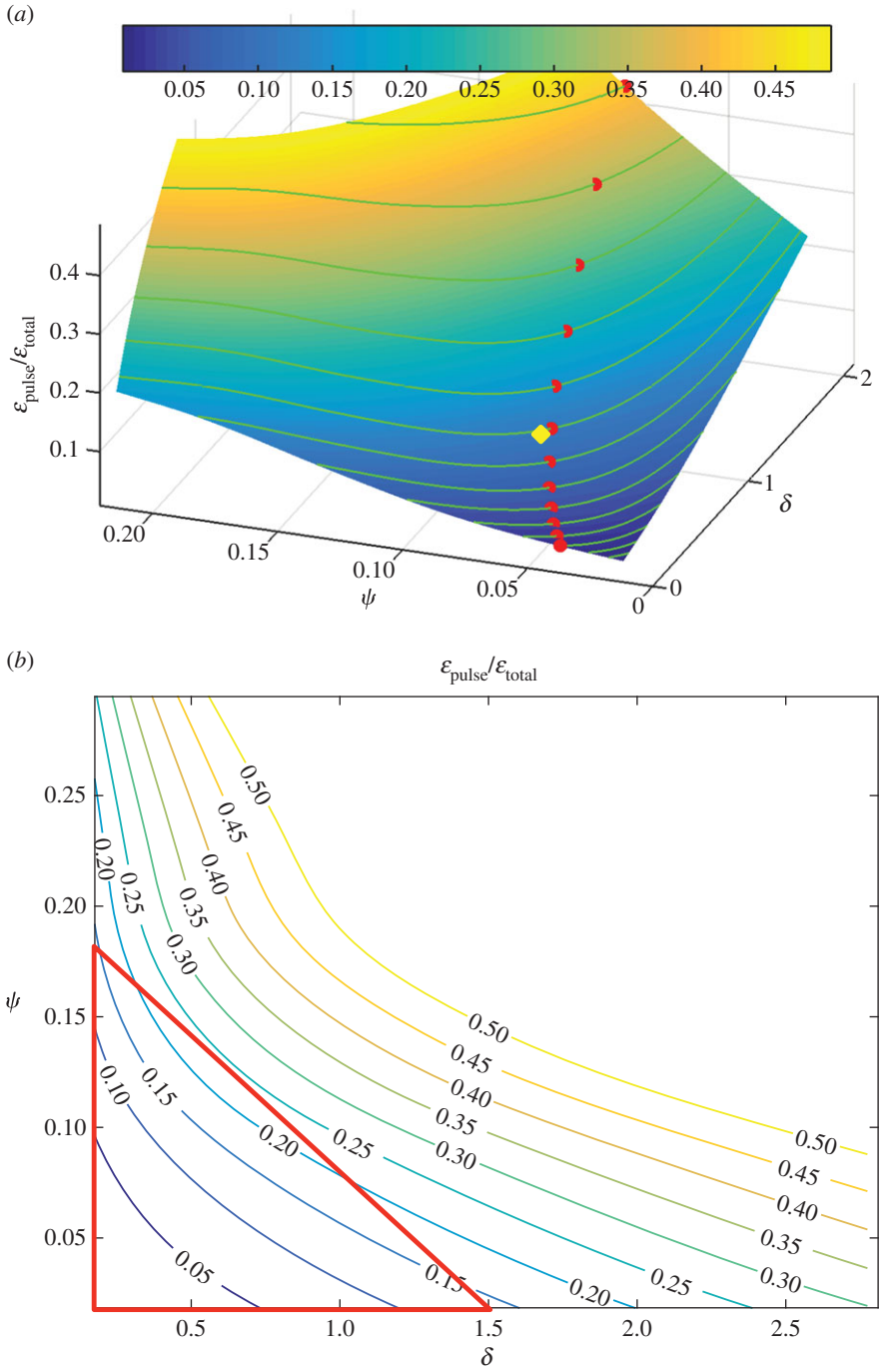

Figure 4. The ratio of pulsatile power loss to total power loss ($\varepsilon_{pulse}/\varepsilon_{total}$) plotted versus changes in propagation number ($\psi = HR\sqrt{L_aC_a}$) and decay number ($\delta = 1/(HRR_pC_T)$) at constant resistance index ($RI = 10^{-9}R_p/(\rho \times CO \times BSA^{-2}) = 3.85$). Baseline condition (yellow marker, diamond) yields $\varepsilon_{pulse}/\varepsilon_{total} = 0.13$ at (δ, ψ) : (0.7, 0.074). (*a*) Surface graph representation. Green curves represent constant vascular states ($\delta \times \psi = const.$), for each vascular state an optimal (δ, ψ) pair is found (red markers, closed circles), where $\varepsilon_{pulse}/\varepsilon_{total}$ is at a local minimum. (*b*) Contour plot representation illustrating the region where the pulsatile energy loss budget is small, i.e. $\psi + 0.12\delta < 0.18$ encloses the region in which $\varepsilon_{pulse}/\varepsilon_{total}$ is approximately below 0.2 (red triangle). The colour legend shown in (*a*) corresponds to $\varepsilon_{pulse}/\varepsilon_{total}$. HR, heart rate; L_a, arterial inertance; C_a, arterial compliance; C_T, total compliance; R_p, peripheral resistance; ρ, blood density; CO, cardiac output; BSA, body surface area.

closed models, activation functions (e.g. ventricular time-varying elastance function), should be given as inputs to the non-dimensionalization function. The final step is the non-dimensionalization of the parameters using the conventions presented in §2.2. Alternatively, for an N compartment circulation network, there are at least N coupled differential equations to solve, after which non-dimensionalization of each equation will lead to the same compartmental non-dimensional number set (not shown here for brevity).

The total ventricular load ($\bar{E}_V$) can be obtained from the sum of the cycle-averaged integral of the pressure–volume loop of each ventricle,

$$\bar{E}_V = \sum \frac{1}{T} \oint p_i \, dV_i, \tag{3.1}$$

where V is the ventricular volume and summation is over all ventricles, as labelled by i. All the power produced by the ventricles is eventually dissipated as heat at the components of the circulatory system, which can be determined individually for each compartment using equations (2.4*a*,*b*). Application of the energy conservation principle, combined with equations (2.4*a*,*b*), determines the energy budget for

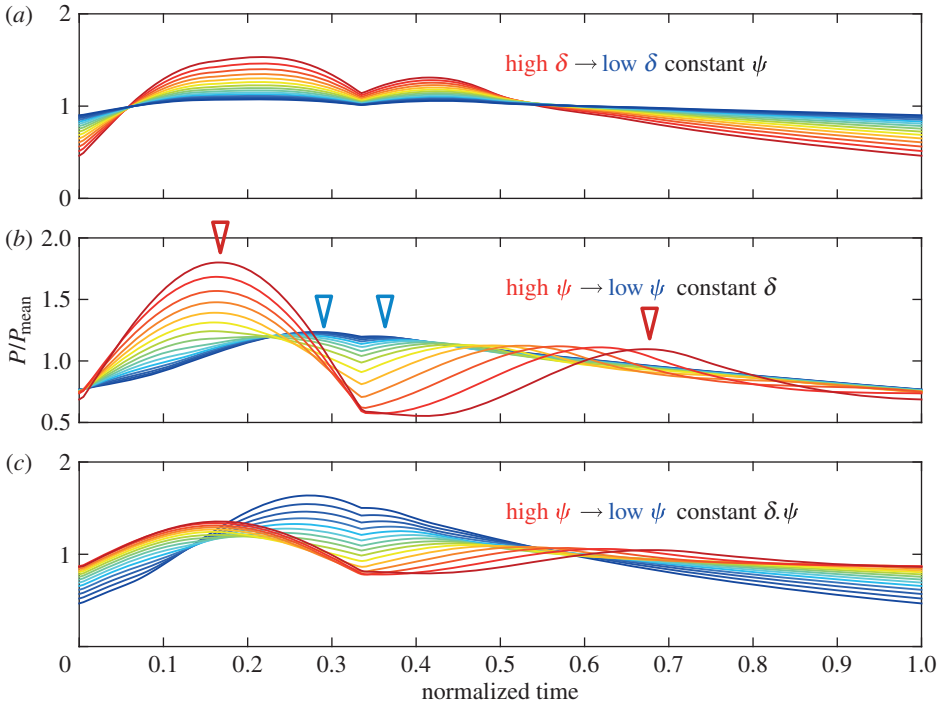

Figure 5. Trends in the pressure waveform sampled at the ventricular–arterial junction due to systematic alterations of cardiovascular non-dimensional parameters. Plots display the changes in the normalized pressure waveform when δ is changed and ψ is fixed in (*a*), ψ is changed and δ is fixed in (*b*), ψ and δ are inversely changed since $\delta \times \psi$ is fixed in (*c*). In (*b*) arrows indicate the separation between the peaks of the forward (transmission) wave and the windkessel wave that closes as ψ decreases. Pressure is normalized with the mean arterial pressure (P/P_{mean}) and time is normalized with the heart rate (HR); normalized time = tHR. δ, decay number; ψ, propagation number.

the entire cardiovascular system as:

$$\begin{aligned}\mathrm{PLI_V} &= \sum_{\text{all compartments}} \mathrm{PLI}_i \\ &= \sum_{\text{lumped}} \alpha_i^2 \mathrm{RI}_i . f_i(\delta_i, \psi_i, Q_{\omega,i}, S_i, \beta_i) \\ &\quad + \sum_{\text{distributed}} \alpha_i^3 \left(\frac{l_i}{\sqrt{\mathrm{BSA}}}\right)^{-4} g_i(Re_i, Ca_i, St_i, Q_{\omega,i}, S_i, \beta_i),\end{aligned} \tag{3.2}$$

where each compartment is labelled by subscript *i*. 'lumped' and 'distributed' indicate that the compartments are defined by the corresponding dimensionless number sets, given by equations (2.2) and (2.3).

In equation (3.2), BCs are assumed individually for all compartments. In fact, if the network connectivity map is known, such as for the circulations in figure 6, with all compartmental information present, then it is sufficient to know the BCs at open boundaries only (there would be no open boundaries for closed networks). For connected compartments, BCs at junctions with neighbouring compartments (i.e. β) and the distribution of flow (i.e. α) will be determined by the properties of the rest of the compartmental network, to which the compartment under investigation is connected, and by the BCs imposed from the open boundaries of the largest connected subgraph. A definitive implication is that local changes in compartmental properties will have global effects. As an example, supposing a network has two compartments, such as arterial and peripheral as shown in §3.1, an increase in stiffness in the arterial compartments would affect power loss in the periphery by altering the flow–pressure waveforms imposed on the microvasculature.

As the number of compartments increases along with increasing model complexity, the quantity of non-dimensional numbers that are required to represent the entire network also increases, because of a larger number of degrees of freedom. Therefore, determining the least number of parameters that can sufficiently define the compartment models, through model reduction and importance analysis, is critical for non-dimensional network analysis [59,60].

4. Discussion

4.1. Energetic implications of non-dimensional parameters

In our earlier studies, it has not been possible to validate the steady non-dimensional energy dissipation scheme of Dasi *et al.* [18] against the empirical allometric relations because of the incomplete non-dimensional number set. This study completed the governing number set by providing a unified picture of the transmission and WK effects on the pulsatile energetic load, and showed that the present generalized non-dimensional set is valid for both steady and pulsatile flow regimes, providing an indirect physical explanation for the cardiovascular allometric observations through physical similitude for the first time in the published literature.

Pulse propagation and reflection characteristics in mammals have been investigated empirically using allometric relations and non-dimensional parameters and have been found to be independent of animal size; however, an explanation for this observation was not previously provided [61]. In a series of papers, Pahlevan & Gharib [62,63] investigated the impact of arterial stiffness, heart rate and wave reflections on the pulsatile power loss. Their study found

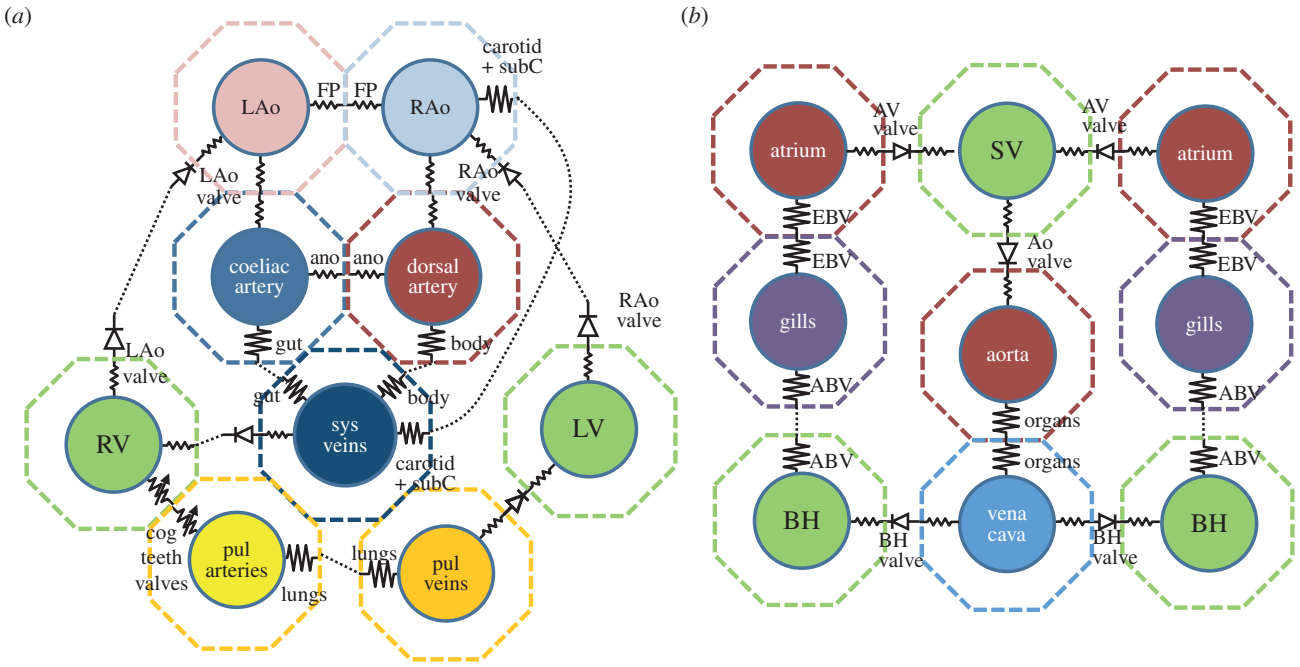

Figure 6. Compartmentalization of two example complex circulatory systems. (*a*) Crocodile circulation network, (*b*) octopus circulation with three isolated ventricles. Individual compartments are shown in hexagonal cells. In this compartmentalization scheme, edges connecting cells consist of a resistance and inertance in series, whereas compliance elements are located on the vertices. Organ or valve resistance and inertances are conceptually shared between the two neighbouring compartments. The multiple inlet and outlets are treated as one combined branch in the governing equations. FP, foramen of Panizza; ano, anastomosis shunt; PVR, lungs; LAo and RAo, left and right aorta, respectively; LV, RV and SV, left, right and single ventricle, respectively; pul and sys, pulmonary and systemic, respectively; subC, subclavian; EBV and ABV, efferent and afferent branchial vessels, respectively; BH, branchial heart, AV, atrio-ventricular; Ao, aortic. (Online version in colour.)

optimality criteria for mammals based on matching the heart rate with the travel time of pulse waves along the aorta to minimize ventricular load [64]. They proposed an invariant wave condition number, which is equal to the product of the heart rate and the effective length of the aorta divided by the pulse wave velocity (PWV), which in turn is equal to 0.1 when the heart rate is optimized. If the effective length is close to the aortic length, as is the case for healthy subjects [65], then the invariant number from Pahlevan and Gharib corresponds directly to the ψ number, as $1/\sqrt{LC}$ is the natural frequency of the aorta and is equal to PWV divided by the aortic length. To account for cases in which the effective length of the aorta differs from its anatomical length, the ratio of the effective length to the anatomical length can be incorporated into S; this allows Pahlevan and Gharib's wave condition number to be obtained by combining S and ψ. Unlike these previous studies, which neglected the damping characteristics of the peripheral circulation, our analysis demonstrated that the ψ number alone does not guarantee optimal cardiac performance, unless the vascular state is fixed. We found that, for each vascular state, the optimal ψ value changes, as well as the corresponding δ value, although the former varies less than the latter.

It is well known that an increase in vascular stiffness impairs pulse buffering by the WK effect and increases the pulse pressure faced by the ventricle [66]. Westerhof & Elzinga [67] reported their observations on the invariance of the product of the heart rate and the arterial pulse decay time of WK3 based on empirical measurements in mammals; their data suggest that $0.2 < \delta < 0.5$. Our study demonstrates that the arterial system operates more efficiently when $\delta < 1$, which suggests that the mammalian peripheral vascular system is adjusted to minimize the pulsatile workload of the ventricle.

Physically, a constant ψ indicates that the spatial and temporal distribution of forward and reflected waves is similar across species, and the constancy of δ implies that the pressure decay during a cardiac cycle is identical. In sum, it is implicitly assumed that the pressure wave faced by the heart during the ejection period is similar for all mammals. This is generally true for most mammals; one exception that is frequently mentioned is the kangaroo, which has an unusual pressure waveform [68]. An inspection of pressure and flow tracings from non-mammalian species showed waveform similarities between tuna [69], turtle [70], alligator [56] and mammals. Through a WK2 parametric estimation, we calculated a $\delta = 0.34 \pm 0.12$ across vertebrate species, where $\delta \sim 0.45$ for active species such as mammals and tuna and $\delta \sim 0.25$ for the less active turtle and alligator. Past experiments on lower vertebrates (toad, lizard and snake) have shown that pulse propagation plays a minor role compared with its role in active animals, as the pulse transit time-to-cardiac cycle duration ratio is significantly lower (5–10 times lower ψ than in mammals, according to [71]) and their arterial system acts mainly as a WK [71]. We suggest that the observed invariance of δ could be valid for lower vertebrates and mammals.

4.2. Implications for achieving optimized states beyond the baseline

From figure 3, it is observed that an additional reduction of pulsatile power loss from the baseline state is possible by decreasing L or increasing C, but these states may not be achieved because of mechanical or physiological design

constraints, such as the limitation on allowed vascular volume or nonlinear dynamic effects. Therefore, in table 3, we summarize the impact of different vascular properties on the power-loss mechanisms governed by linear flow effects through the main findings of this paper, and discuss nonlinear effects that are not included in the linear model, such as steep wavefronts and turbulence. Considering that ρ and μ are relatively constant, increasing aortic luminal area (A_0) or decreasing vascular elastic modulus represent the available options to decrease power loss by obtaining a smaller R, L and a larger C, as traced in figure 3. However, increasing A_0 requires a larger blood volume; while, on the other hand, decreasing E might lead to a low PWV, resulting in the occurrence of nonlinear steep wavefronts, if the flow velocity approaches PWV. Therefore, these two factors may impose a lower limit to the reduction of pulsatile energetic load. Strain-stiffening elasticity is another nonlinear effect, but it only contributes to a higher power loss when blood pressure is high, which necessitates an already high power loss. Thus, it is not expected to constitute a limiting factor in the low-power design.

4.3. Relation between lumped and distributed non-dimensional parameters

Equations (2.2) and (2.3) are applicable in both steady and pulsatile flow regimes. Under steady flow, δ and ψ as well as Q_ω vanish, and the PLI becomes a function of RI and S alone (pulsatile power loss is replaced by steady power loss). The framework proposed in Dasi *et al.* [18] and ours, proposed here, can be linked using the Darcy–Weisbach equation for pressure loss, which is a function of the Darcy friction factor f_D, pipe length l and diameter d, mean flow velocity u and fluid density ρ: $\Delta P = f_D \times \frac{L}{D} \times \frac{\rho u^2}{2}$. As resistance is the ratio of mean pressure drop to the mean flow rate, its functional dependence is identical to the Darcy–Weisbach equation for pressure loss: $\Delta P/Q = R = f(f_D, L, D, u, \rho)$. Non-dimensionalization of this expression returns RI and its functional dependence on f_D and L/D as $R/(\rho Q/D^4) = f(f_D, L/D)$. Considering pipe flow, f_D can be determined empirically from the Moody chart, if the Reynolds number and the surface roughness are known. Thus, the definition of PLI as a function of RI is identical to its definition based on Re: $\mathrm{PLI} = f(RI, S) \equiv f(Re, S)$.

As explained in §4.1, ψ is equivalent to the ratio of arterial length to the distance travelled by a pulse wave in the duration of a cardiac cycle

$$\mathrm{HR}\sqrt{LC} = \frac{\mathrm{HR}l}{\mathrm{PWV}}.$$

PWV can be estimated with the Moens–Korteweg formula: $\mathrm{PWV} = \sqrt{(Eh/\rho d)}$, where h and d are wall thickness and internal diameter [39], respectively. Thus, the ψ number is identical to

$$\frac{\mathrm{HR}l}{\sqrt{Eh/\rho d}} = \frac{St}{\sqrt{Ca}\sqrt{h/d}},$$

with characteristic length chosen as the longitudinal vascular length and h/d is the shape number. The δ number governs the frequency-dependent interaction of viscous fluid and elastic wall forces. Combining Re, Ca, St and S numbers gives an identical relation:

$$\delta \equiv \left(\frac{E}{\mathrm{HR}.\mu}, S\right) = \left(\frac{Re.Ca}{St}, S\right).$$

This emphasizes the compatibility of the proposed lumped parameter description of power loss to its distributed parameter description that was derived in §2.2.

4.4. Inertial and viscous scaling

From equations (2.4*a*,*b*), it is observed that mean power loss should be proportional to the cube of the flow rate in order for PLI to remain insensitive to variations in the mean flow rate. This relation is valid for cardiovascular segments where energy dissipation is dominated by inertial losses under high-Re conditions. However, under laminar flow regimes ($Re < 2000$–3000), viscous forces dominate energy dissipation and the power-loss dependency on flow rate becomes a quadratic function of the flow rate ($\varepsilon \propto Q^2$). It is important to make this distinction, as most power loss in the cardiovascular system occurs at the level of the microcirculation, where viscous forces are dominant. Equations (2.4*a*,*b*) can be adjusted to a suitable form for flow regimes that are dominated by viscous forces by simply multiplying the left-hand side by the Reynolds number as:

$$\frac{\varepsilon_p}{\mu(\bar{Q}^2/\mathrm{BSA}^{3/2})} = \mathrm{RI}_\mu f(\delta, \psi, Q_\omega, S, \beta) = Reg(Re, Ca, St, Q_\omega, S, \beta), \quad (4.1)$$

where $\mathrm{RI}_\mu = R/\mu BSA^{-3/2}$ is the viscosity-scaled resistance index.

4.5. Non-dimensional numbers in the clinical setting

Flow pulsatility has been shown to be beneficial for organ perfusion [27] as well as healthy vascular gene expression and remodelling; however, the energetic cost of delivering a constant CO is higher in pulsatile flow than in non-pulsatile flow [26,72]. In the healthy circulatory system, the pulsatile component of ventricular load operates optimally and constitutes a small fraction of the total power requirement of the ventricle (approx. 10%). However, many diseases, including congestive heart failure, ventricular hypertrophies, adverse vascular remodelling and congenital heart disease, as well as cardiovascular device performance (neonatal CPB, ventricle assist devices), are closely associated with increased pulsatile workload on the ventricle. Changes in the cardiovascular system that accompany such diseases were displayed as parametric variations in figure 3.

From the clinical perspective, surface-area scaling is commonly adopted for human physiology [35]; therefore, the PLI can be established as a size-invariant measure of cardiovascular performance. If quarter-power scaling is considered for humans, then a 10-fold variation in size (e.g. 10–100 kg) introduces a 30% variation in PLI between the two extremes of human size, which is still smaller than the variations in PLI introduced by disease conditions [18]. Therefore, the $\mathrm{PLI} \propto M^{-1/6}$ relation that occurs in quarter-power scaling would only cause a weak body-size dependence of PLI when used as a performance index.

As discussed above, decay and propagation numbers correspond directly to the physical properties of the arterial system. Arterial pressure decay time is commonly associated with WK properties, which are determined by total arterial compliance and peripheral resistance. Characteristic arterial decay time ($\tau = RC$) is calculated by estimating the negative of the slope of the diastolic pressure decay curve [73]. We

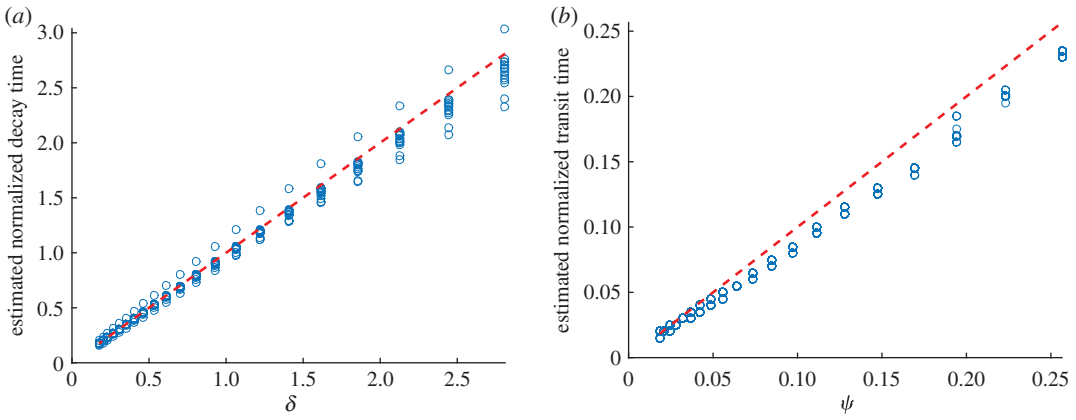

Figure 7. Correlation of non-dimensional parameters with the physical measures estimated from the resulting arterial pressure waveforms as explained in §4.5. (*a*) The decay number correlates well with the normalized decay time of windkessel (=HRτ). Decay time of windkessel is estimated from the slope of the diastolic arterial pressure waveform. (*b*) Propagation number correlates with the normalized arterial pulse transit time (=HR × PTT). PTT is the time it takes for a pulse wave to travel from the aortic inlet to the end of the aorta (reflection site), and is estimated with the foot-to-foot method. Markers (open circles) are the estimated measures (*y*-axis) at each known non-dimensional number value in simulations (*x*-axis). Dashed lines represent a linear relation between measured indices and non-dimensional parameters. HR, heart rate; τ, windkessel decay time; PTT, pulse transit time. (Online version in colour.)

note that δ is different from the *RC* time used in the estimation of total arterial compliance [73]. The value of *RC* time varies with the size of the subject, whereas δ is a scale-invariant index that indicates the WK performance, as it reflects the synchronization of heart rate with the decay properties of the vascular system. Similarly, ψ is shown to be proportional to the normalized transit time of pulse waves from the aortic inlet to the microcirculation boundary, where transit time was estimated using the foot-to-foot method [74].

Figure 7*a*,*b* shows that there is a strong one-to-one association between the normalized decay time and normalized transit time, estimated from the simulated pressure waveforms and the non-dimensional δ and ψ numbers given as inputs to the system. Estimated measures can be used directly to determine the state of the cardiovascular system, the ventricular–arterial coupling and the arterial pressure waveforms by referring to figures 3–5, without having to determine individual values of compliance and inertance.

4.6. Further limitations

The numerical model presented in this paper is the minimum model that is able to capture the transmission and WK properties of the circulation system. In the future, a distributed model of the circulation system may be tested against the present results. Linear models sufficiently capture the dynamics of circulation, however several advanced features may be included in future investigations. For example, nonlinear elasticity and viscoelasticity of the vessels, and inertial power losses, were not incorporated in the present model. Possible impacts of nonlinear effects are discussed in §4.2. Another limitation was that CO and flow waveforms were fixed. For advanced analysis of arterio-ventricular coupling, ventricular time-varying elastance or multi-physics models could be added [75–77].

At present, our model focused on a one inlet–one outlet transmission-WK model. However, vascular systems feature more complex branches with multiple inlets and outlets (e.g. carotid bifurcation (one inlet, two outlets), aortic arch (one inlet, four outlets), venous confluence (two inlets, one outlet) and hepatic confluence (three inlets, one outlet)), with fixed flow and pressure BCs as well as more complex BCs, which are determined by upstream and downstream vascular structures. For a more general power loss estimation, improved impedance calculations using the reduced-order, variable morphometric and fractal approaches [78–80] will be considered.

5. Conclusion

A complete set of non-dimensional numbers that govern both the steady and the pulsatile physics of cardiovascular systems are formulated. Non-dimensionalization of both lumped and distributed models of circulation is studied, covering the individual cardiovascular components as well as entire networks. Non-dimensional parameters obtained from a lumped arterial circulation model yield invariant characteristics, which were derived from common design principles of the circulatory systems of animals. We used the non-dimensionalization framework to elucidate the determinants of pulsatile load in the arterial system with a reduced number of variables. For the first time in the published literature, the complete optimal state maps of arterial circulation systems are calculated and the relative importance of pulsatile versus steady cardiovascular energy is quantified. The determinant non-dimensional variables governing decay and propagation characteristics can be acquired from the subject-specific routine clinical measurements, and would allow comparative assessment of optimal cardiovascular states. Extension of the presented framework towards the scaling of complex circulatory networks was also considered. Similitude of cardiovascular function across species will be useful in network optimization, as the only variable among the circuit candidates will be their 'network topology', allowing unbiased comparison of non-dimensional energetics and efficiency parameters.

Authors' contributions. The authors contributed equally to the study design and manuscript.

Competing interests. We declare we have no competing interests.

Funding. Funding was provided by European Research Council (ERC) grant no. 307460, Marie Curie FP7 293931 CardioFluidMechanics and National Science Foundation CAREER award no. 0954465.

References

1. Vogel S. 1994 Nature's pumps. *Am. Sci.* **82**, 464–471.
2. Kilner PJ, Yang G-Z, Firmin DN. 2001 Morphodynamics of flow through sinuous curvatures of the heart. *Biorheology* **39**, 409–417.
3. Wood S. 1984 Cardiovascular shunts and oxygen transport in lower vertebrates. *Am. J. Physiol. Regul. Integr. Compar. Physiol.* **247**, R3–R14.
4. Sturkie PD, Dirner G, Gister R. 1977 Shunting of blood from the renal portal to the hepatic portal circulation in chickens. *Compar. Biochem. Physiol. A* **58**, 213–215. (doi:10.1016/0300-9629(77)90228-6)
5. Bergwer VM, DeRuiter M, Gittenberger-de Groot A. 1999 Comparative anatomy and ontogeny of the ductus arteriosus, a vascular outsider. *Anat. Embryol.* **200**, 559–571. (doi:10.1007/s004290050304)
6. Bourne GB. 1984 Pressure-flow relationships in the perfused post-systemic circulation of the squid, *Loligo pealei*. *Compar. Biochem. Physiol. A* **78**, 307–313. (doi:10.1016/0300-9629(84)90152-X)
7. Houlihan DF, Agnisola C, Hamilton NM, Genoino T. 1987 Oxygen consumption of the isolated heart of octopus: effects of power output and hypoxia. *J. Exp. Biol.* **131**, 137–157.
8. Shadwick RE, Nilsson EK. 1990 The importance of vascular elasticity in the circulation system of the cephalopod *Octopus vulgaris*. *J. Exp. Biol.* **152**, 471–484.
9. Franklin CE, Axelsson M. 2000 Physiology: an actively controlled heart valve. *Nature* **406**, 847–848. (doi:10.1038/35022652)
10. Burggren W. 1988 Cardiac design in lower vertebrates: what can phylogeny reveal about ontogeny? *Experientia* **44**, 919–930. (doi:10.1007/BF01939885)
11. Burggren WW, Pinder AW. 1991 Ontogeny of cardiovascular and respiratory physiology in lower vertebrates. *Annu. Rev. Physiol.* **53**, 107–135. (doi:10.1146/annurev.ph.53.030191.000543)
12. Burggren WW, Keller BB. 1997 *Development of cardiovascular systems: molecules to organisms*. Cambridge, UK: Cambridge University Press.
13. Forster MF. 1997 The blood sinus system of hagfish: its significance in a low-pressure circulation. *Compar. Biochem. Physiol. A* **116**, 123–244. (doi:10.1016/S0300-9629(96)00215-0)
14. Brand AR. 1972 The mechanism of blood circulation in *Anodonta anatina*. *J. Exp. Biol.* **56**, 361–379.
15. Florey E, Cahill MA. 1977 Hemodynamics in lamellibranch molluscs: confirmation of constant-volume mechanism of auricular and ventricular filling. Remarks on the heart as site of ultrafiltration. *Compar. Biochem. Physiol. A* **57**, 47–52. (doi:10.1016/0300-9629(77)90347-4)
16. Blasius H. 1911 The similarity law in friction processes. *Physik. Z.* **12**, 1175–1177.
17. Buckingham E. 1914 On physically similar systems, illustrations of the use of dimensional equations. *Phys. Rev.* **4**, 345–376. (doi:10.1103/PhysRev.4.345)
18. Dasi LP, Pekkan K, de Zelicourt D, Sundareswaran KS, Krishnankutty R, Delnido PJ, Yoganathan AP. 2009 Hemodynamic energy dissipation in the cardiovascular system: generalized theoretical analysis on disease states. *Ann. Biomed. Eng.* **37**, 661–673. (doi:10.1007/s10439-009-9650-0)
19. Dasi LP, Pekkan K, Katajima HD, Yoganathan AP. 2008 Functional analysis of Fontan energy dissipation. *J. Biomech.* **41**, 2246–2252. (doi:10.1016/j.jbiomech.2008.04.011)
20. Dasi LP *et al.* 2009 Fontan hemodynamics: importance of pulmonary artery diameter. *J. Thorac. Cardiovasc. Surg.* **137**, 560–564. (doi:10.1016/j.jtcvs.2008.04.036)
21. Phillips C, Simon-Walker RL, Dasi LP. 2014 Energy costs of singular and concomitant pressure and volume overload lesions. *Cardiovasc. Eng. Technol.* **5**, 44–53. (doi:10.1007/s13239-013-0173-3)
22. Safar ME, Levy BI, Struijker-Boudier H. 2003 Current perspectives on arterial stiffness and pulse pressure in hypertension and cardiovascular diseases. *Circulation* **107**, 2864–2869. (doi:10.1161/01.CIR.0000069826.36125.B4)
23. Mitchell GF, Tardif J-C, Arnold JMO, Marchiori G, O'Brien TX, Dunlap ME, Pfeffer MA. 2001 Pulsatile hemodynamics in congestive heart failure. *Hypertension* **38**, 1433–1439. (doi:10.1161/hy1201.098298)
24. Pekkan K, Dur O, Sundareswaran K, Kanter K, Fogel M, Yoganathan A, Undar A. 2008 Neonatal aortic arch hemodynamics and perfusion during cardiopulmonary bypass. *J. Biomech. Eng.* **130**, 061012. (doi:10.1115/1.2978988)
25. Khiabani RH, Whitehead KK, Han D, Restrepo M, Tang E, Bethel J, Paridon SM, Fogel MA, Yoganathan AP. 2014 Exercise capacity in single-ventricle patients after Fontan correlates with haemodynamic energy loss in TCPC. *Heart* **101**, 139–143. (doi:10.1136/heartjnl-2014-306337)
26. Ündar A, Masai T, Frazier O, Fraser Jr CD. 1999 Pulsatile and nonpulsatile flows can be quantified in terms of energy equivalent pressure during cardiopulmonary bypass for direct comparisons. *ASAIO J.* **45**, 610–614. (doi:10.1097/00002480-199911000-00017)
27. Ündar A, Masai T, Yang S-Q, Goddard-Finegold J, Frazier O, Fraser CD. 1999 Effects of perfusion mode on regional and global organ blood flow in a neonatal piglet model. *Ann. Thorac. Surg.* **68**, 1336–1342. (doi:10.1016/S0003-4975(99)00913-3)
28. Santhanakrishnan A, Maher KO, Tang E, Khiabani RH, Johnson J, Yoganathan AP. 2013 Hemodynamic effects of implanting a unidirectional valve in the inferior vena cava of the Fontan circulation pathway: an in vitro investigation. *Am. J. Physiol. Heart Circ. Physiol.* **305**, H1538–H1547. (doi:10.1152/ajpheart.00351.2013)
29. Yap CH, Dasi LP, Yoganathan AP. 2010 Dynamic hemodynamic energy loss in normal and stenosed aortic valves. *J. Biomech. Eng.* **132**, 021005. (doi:10.1115/1.4000874)
30. Khiabani RH, Restrepo M, Tang E, de Zélicourt D, Sotiropoulos F, Fogel M, Yoganathan AP. 2012 Effect of flow pulsatility on modeling the hemodynamics in the total cavopulmonary connection. *J. Biomech.* **45**, 2376–2381. (doi:10.1016/j.jbiomech.2012.07.010)
31. Tang E, Haggerty CM, Khiabani RH, de Zélicourt D, Kanter J, Sotiropoulos F, Fogel MA, Yoganathan AP. 2013 Numerical and experimental investigation of pulsatile hemodynamics in the total cavopulmonary connection. *J. Biomech.* **46**, 373–382. (doi:10.1016/j.jbiomech.2012.11.003)
32. Shepard RB, Simpson DC, Sharp JF. 1966 Energy equivalent pressure. *Arch. Surg.* **93**, 730–740. (doi:10.1001/archsurg.1966.01330050034005)
33. Dewey FE, Rosenthal D, Murphy Jr DJ, Froelicher VF, Ashley EA. 2008 Does size matter? Clinical applications of scaling cardiac size and function for body size. *Circulation* **117**, 2279–2287. (doi:10.1161/CIRCULATIONAHA.107.736785)
34. van de Vosse FN, Stergiopulos N. 2011 Pulse wave propagation in the arterial tree. *Annu. Rev. Fluid Mech.* **43**, 467–499. (doi:10.1146/annurev-fluid-122109-160730)
35. Sluysmans T, Colan SD. 2005 Theoretical and empirical derivation of cardiovascular allometric relationships in children. *J. Appl. Physiol.* **99**, 445–457. (doi:10.1152/japplphysiol.01144.2004)
36. Holt J, Rhode E, Holt W, Kines H. 1981 Geometric similarity of aorta, venae cavae, and certain of their branches in mammals. *Am. J. Physiol.* **241**, R100–R104.
37. Westerhof BE, van den Wijngaard JP, Murgo JP, Westerhof N. 2008 Location of a reflection site is elusive consequences for the calculation of aortic pulse wave velocity. *Hypertension* **52**, 478–483. (doi:10.1161/HYPERTENSIONAHA.108.116525)
38. Murgo JP, Westerhof N, Giolma JP, Altobelli SA. 1980 Aortic input impedance in normal man: relationship to pressure wave forms. *Circulation* **62**, 105–116. (doi:10.1161/01.CIR.62.1.105)
39. Fung Y-C. 1997 *Biomechanics: circulation*. Berlin, Germany: Springer.
40. Zamir M. 2000 *The physics of pulsatile flow*. Berlin, Germany: Springer.
41. Alastruey J, Siggers JH, Peiffer V, Doorly DJ, Sherwin SJ. 2012 Reducing the data: analysis of the role of vascular geometry on blood flow patterns in curved vessels. *Phys. Fluids* **24**, 031902. (doi:10.1063/1.3694526)
42. Mynard JP, Valen-Sendstad K. 2015 A unified method for estimating pressure losses at vascular junctions. *Int. J. Numer. Methods Biomed. Eng.* **31**, e02717. (doi:10.1002/cnm.2717)
43. West GB, Brown JH, Enquist BJ. 1997 A general model for the origin of allometric scaling laws in biology. *Science* **276**, 122–126. (doi:10.1126/science.276.5309.122)

44. Banavar JR, Maritan A, Rinaldo A. 1999 Size and form in efficient transportation networks. *Nature* **399**, 130–132. (doi:10.1038/20144)
45. Banavar JR, Moses ME, Brown JH, Damuth J, Rinaldo A, Sibly RM, Maritan A. 2010 A general basis for quarter-power scaling in animals. *Proc. Natl Acad. Sci. USA* **107**, 15 816–15 820. (doi:10.1073/pnas.1009974107)
46. Banavar JR, Cooke TJ, Rinaldo A, Maritan A. 2014 Form, function, and evolution of living organisms. *Proc. Natl Acad. Sci. USA* **111**, 3332–3337. (doi:10.1073/pnas.1401336111)
47. Schmidt-Nielsen K. 1984 *Scaling: why is animal size so important?* Cambridge, UK: Cambridge University Press.
48. Li JK. 1995 *Comparative cardiovascular dynamics of mammals*. Boca Raton, FL: CRC Press.
49. Baskurt OK, Meiselman HJ. 2013 Comparative hemorheology. *Clin. Hemorheol. Microcirc.* **53**, 61–70.
50. Shadwick RE. 1999 Mechanical design in arteries. *J. Exp. Biol.* **202**, 3305–3313.
51. Georgakopoulos D, Mitzner WA, Chen CH, Byrne BJ, Millar HD, Hare JM, Kass DA. 1998 *In vivo* murine left ventricular pressure-volume relations by miniaturized conductance micromanometry. *Am. J. Physiol.* **274**, H1416–H1422.
52. O'Rourke MF. 1967 Steady and pulsatile energy losses in the systemic circulation under normal conditions and in simulated arterial disease. *Cardiovasc. Res.* **1**, 313–326. (doi:10.1093/cvr/1.4.313)
53. Otsuki T, Maeda S, Iemitsu M, Saito Y, Tanimura Y, Ajisaka R, Miyauchi T. 2008 Systemic arterial compliance, systemic vascular resistance, and effective arterial elastance during exercise in endurance-trained men. *Am. J. Physiol.* **295**, R228–R235. (doi:10.1152/ajpregu.00009.2008)
54. Sharman J, McEniery C, Campbell R, Coombes J, Wilkinson I, Cockcroft J. 2005 The effect of exercise on large artery haemodynamics in healthy young men. *Eur. J. Clin. Investig.* **35**, 738–744. (doi:10.1111/j.1365-2362.2005.01578.x)
55. Mohiuddin MW, Laine GA, Quick CM. 2007 Increase in pulse wavelength causes the systemic arterial tree to degenerate into a classical windkessel. *Am. J. Physiol.* **293**, H1164–H1171. (doi:10.1152/ajpheart.00133.2007)
56. Shelton G, Jones D. 1991 The physiology of the alligator heart: the cardiac cycle. *J. Exp. Biol.* **158**, 539–564.
57. Axelsson M, Holm S, Nilsson S. 1989 Flow dynamics of the crocodilian heart. *Am. J. Physiol.* **256**, R875–R879.
58. Wells M, Smith P. 1987 The performance of the octopus circulatory system: a triumph of engineering over design. *Experientia* **43**, 487–499. (doi:10.1007/BF02143577)
59. Kittirungsi B. 2008 *A scaling methodology for dynamic systems: quantification of approximate similitude and use in multiobjective design*, p. 132. Ann Arbor, MI: ProQuest.
60. Ersal T, Kittirungsi B, Fathy HK, Stein JL. 2009 Model reduction in vehicle dynamics using importance analysis. *Vehicle Syst. Dyn.* **47**, 851–865. (doi:10.1080/00423110802444071)
61. Li JK, Noordergraaf A. 1991 Similar pressure pulse propagation and reflection characteristics in aortas of mammals. *Am. J. Physiol.* **261**, R519–R521.
62. Pahlevan NM, Gharib M. 2011 Aortic wave dynamics and its influence on left ventricular workload. *PLoS ONE* **6**, e23106. (doi:10.1371/journal.pone.0023106)
63. Pahlevan NM, Gharib M. 2014 A bio-inspired approach for the reduction of left ventricular workload. *PLoS ONE* **9**, e87122. (doi:10.1371/journal.pone.0087122).
64. Pahlevan NM, Gharib M. 2014 A wave dynamics criterion for optimization of mammalian cardiovascular system. *J. Biomech.* **47**, 1727–1732. (doi:10.1016/j.jbiomech.2014.02.014)
65. Segers P, Rietzschel ER, De Buyzere ML, De Bacquer D, Van Bortel LM, De Backer G, Gillebert TC, Verdonck PR. 2007 Assessment of pressure wave reflection: getting the timing right!. *Physiol. Meas.* **28**, 1045. (doi:10.1088/0967-3334/28/9/006)
66. Stergiopulos N, Westerhof N. 1998 Determinants of pulse pressure. *Hypertension* **32**, 556–559. (doi:10.1161/01.HYP.32.3.556)
67. Westerhof N, Elzinga G. 1991 Normalized input impedance and arterial decay time over heart period are independent of animal size. *Am. J. Physiol.* **261**, R126–R133.
68. Nichols WW, Avolio AP, O'Rourke MF. 1986 Ascending aortic impedance patterns in the kangaroo: their explanation and relation to pressure waveforms. *Circ. Res.* **59**, 247–255. (doi:10.1161/01.RES.59.3.247)
69. Jones DR, Brill RW, Bushnell PG. 1993 Ventricular and arterial dynamics of anaesthetised and swimming tuna. *J. Exp. Biol.* **182**, 97–112.
70. Hicks JW, Ishimatsu A, Molloi S, Erskin A, Heisler N. 1996 The mechanism of cardiac shunting in reptiles: a new synthesis. *J. Exp. Biol.* **199**, 1435–1446.
71. Gibbons C, Shadwick R. 1989 Functional similarities in the mechanical design of the aorta in lower vertebrates and mammals. *Experientia* **45**, 1083–1088. (doi:10.1007/BF01950164)
72. Ündar A, Eichstaedt HC, Masai T, Yang S-Q, Bigley JE, McGarry MC, Mueller M, Vaughn WK, Fraser Jr CD. 2001 Comparison of six pediatric cardiopulmonary bypass pumps during pulsatile and nonpulsatile perfusion. *J. Thoracic Cardiovasc. Surg.* **122**, 827–829. (doi:10.1067/mtc.2001.114931)
73. Stergiopulos N, Meister J, Westerhof N. 1995 Evaluation of methods for estimation of total arterial compliance. *Am. J. Physiol.* **268**, H1540–H1548.
74. Nichols W, O'Rourke M, Vlachopoulos C. 2011 *McDonald's blood flow in arteries: theoretical, experimental and clinical principles*. Boca Raton, FL: CRC Press.
75. Suga H, Sagawa K, Shoukas AA. 1973 Load independence of the instantaneous pressure-volume ratio of the canine left ventricle and effects of epinephrine and heart rate on the ratio. *Circ. Res.* **32**, 314–322. (doi:10.1161/01.RES.32.3.314)
76. Kerckhoffs RC, Neal ML, Gu Q, Bassingthwaighte JB, Omens JH, McCulloch AD. 2007 Coupling of a 3D finite element model of cardiac ventricular mechanics to lumped systems models of the systemic and pulmonic circulation. *Ann. Biomed. Eng.* **35**, 1–18. (doi:10.1007/s10439-006-9212-7)
77. Nordsletten D, Niederer S, Nash M, Hunter P, Smith N. 2011 Coupling multi-physics models to cardiac mechanics. *Prog. Biophys. Mol. Biol.* **104**, 77–88. (doi:10.1016/j.pbiomolbio.2009.11.001)
78. Spilker RL, Feinstein JA, Parker DW, Reddy VM, Taylor CA. 2007 Morphometry-based impedance boundary conditions for patient-specific modeling of blood flow in pulmonary arteries. *Ann. Biomed. Eng.* **35**, 546–559. (doi:10.1007/s10439-006-9240-3)
79. Du T, Hu D, Cai D. 2015 Outflow boundary conditions for blood flow in arterial trees. *PLoS ONE* **10**, e0128597. (doi:10.1371/journal.pone.0128597)
80. Vignon-Clementel IE, Figueroa CA, Jansen KE, Taylor CA. 2006 Outflow boundary conditions for three-dimensional finite element modeling of blood flow and pressure in arteries. *Comput. Methods Appl. Mech. Eng.* **195**, 3776–3796. (doi:10.1016/j.cma.2005.04.014)